Numerical solutions for rotating flow of viscoelastic fluid with heat and mass transfer effects

by

Najwa Maqsood

A thesis submitted in partial fulfillment of the requirements

for the degree of Master of Science in Mathematics

Supervised by

Dr. Meraj Mustafa Hashmi

School of Natural Sciences,

National University of Sciences and Technology,

Islamabad, Pakistan

2017

National University of Sciences & Technology

MASTER'S THESIS WORK

We hereby recommend that the dissertation prepared under our supervision by: Ms. Najwa Maqsood, Regn No. 00000117281 Titled: Numerical solutions for rotating flows of viscoelastic fluid with heat and mass transfer effects be accepted in partial fulfillment of the requirements for the award of **MS** degree.

Examination Committee Members

1. Name: Dr. Muhammad Asif Farooq   Signature: _____

2. Name: Dr. Mujeeb ur Rehman   Signature: _____

3. Name: _____   Signature: _____

4. Name: Dr. Masood Khan   Signature: _____

Supervisor's Name: Dr. Meraj Mustafa Hashmi   Signature: _____

_____
Head of Department

09/08/17
Date

COUNTERSINGED

_____
Dean/Principal

Date: 09/8/17

THESIS ACCEPTANCE CERTIFICATE

Certified that final copy of MS thesis written by **Ms. Najwa Maqsood**, (Registration No. **00000117281**), of **School of Natural Sciences** has been vetted by undersigned, found complete in all respects as per NUST statutes/regulations, is free of plagiarism, errors, and mistakes and is accepted as partial fulfillment for award of MS/M.Phil degree. It is further certified that necessary amendments as pointed out by GEC members and external examiner of the scholar have also been incorporated in the said thesis.

Signature: _____

Name of Supervisor <u>Dr. Meraj Mustafa Hashmi</u>

Date: _____09-08-2017_____

Signature (HoD): _____

Date: _____09/08/17_____

Signature (Dean/Principal): _____

Date: _____09/8/17_____

CONTENTS

Abstract

The analysis of fluid flow in a rotating frame has been an active area of research for years. It is of great importance in many engineering, scientific and geophysical applications such as rotating machinery, water turbines, gas turbine designs, pumps, jet engines etc. Maxwell fluid is a common viscoelastic model that can predict stress relaxation phenomenon. Some examples of Maxwell fluid include polymer solutions, toothpaste, ketchup, blood, shampoos and paints. Here, we study heat/mass transfer effects on the viscoelastic fluid flow in rotating frame. The cases of linear and exponential deformation of the boundary are separately discussed. Heat transfer due to non-linear radiation is modeled and deliberated. Mass transfer analysis is carried out in the existence of homogeneous-heterogeneous reactions. Numerical solutions of the developed non-linear problem are obtained by means of shooting method. For a check, the computations are also performed by contemporary tool for solving boundary value problems namely bvp4c of MATLAB. We found that angular velocity of the rotating fluid substantially influence the solution profiles. Velocity fields are oscillatory decaying functions of the non-dimensional vertical distance when fluid is subjected to larger rotation rate. Solute concentration at the surface is highly influenced by varying the strengths of chemical reactions.

Chapter 1

Introduction

This chapter covers some basic definitions and fundamental concepts. A detailed literature review concerning the problems reported in subsequent chapters is presented. Equations governing the motion of Maxwell fluid with heat and mass transfer are also derived.

1.1Background

There is a certain class of materials called non-Newtonian fluids in which the viscosity is a function of shear rate. Representative examples are polymer solutions, molten plastics, food products, emulsions of water in oil, fibers in a liquid paper pulp etc. Viscoelastic fluids are special non-Newtonian fluids which exhibit both viscous and elastic responses to the deforming force that is, they have ability to store and recover shear energy. Maxwell fluid is a common viscoelastic model that can predict stress relaxation phenomenon for many polymer liquids. As a consequence, special attention is devoted to explore boundary layer problems concerning Maxwell fluid. Forced convection heat transfer in Maxwell fluid flow past a non-isothermal deforming sheet was addressed by Vajravelu et al. [1] through a numerical approach. Buoyancy assisting or opposing flow of Maxwell fluid near a stagnation point on vertical stretchable surface was numerically explored by Hsiao [2]. Characteristics of heat transfer in Maxwell fluid flow caused by unsteady deforming boundary were elucidated by Mukhopadhyay [3] via numerical approach. Hayat et al. [4] discussed heat transfer originating from melting process of a stretchable surface immersed in a hot Maxwell fluid. Shehzad et al. [5] investigated two different heating processes for three-dimensional flow of MHD Maxwell fluid. Kumari and Nath [6] modeled the Maxwell fluid flow which results due to exponentially deforming vertical surface with prescribed surface temperature. Ohmic heating effect in stagnation-point flow of Maxwell fluid with buoyancy force effects was analyzed by Hsiao [7]. Khan et al. [8] described

exponentially deforming surface induced flow of viscoelastic Maxwell fluid in the framework of Cattaneo-Christov heat flux theory. Natural convection flow of Maxwell nanofluid with Brownian diffusion and thermophoresis was explored by Mustafa and Mushtaq [9]. In recent years, considerable research in this area has been published (see, for instance, [10-19] and refs. there in).

Rotating flow problems have essence in broad ranging engineering, scientific and geophysical applications such as rotating machinery, jet engines, pumps, gas turbine designs, vacuum cleaner etc. Nowadays, rotating flows around continuously deforming surfaces has attracted considerable attention. The first ever article in this domain was published by Wang [20] who considered the fluid flow over a stretching sheet in a rotating fluid. He presented a similarity solution of developed problem by means of perturbation in small rotation rate. Later, Nazar et al. [21] extended Wang's analysis for unsteady case and provided numerical approximations of velocity profiles through Keller-box method. Asymptotic solutions for large time t have also been derived in this paper. Kumari et al. [22] investigated the rotating flow of non-newtonian Power-Law fluid over a stretching surface. Javed et al. [23] provided locally similar numerical solutions for viscous fluid flow over an exponentially deforming surface in rotating frame. Zaimi et al. [24] made use of Keller-box approach to analyze viscoelastic fluid flow in rotating frame bounded by a stretchable surface. Turkyilmazoglu [25] examined consequences of radial stretching in the Von Karman swirling flow problem of infinite disk. He justified usefulness of radial stretching in terms of heat transfer enhancement via through analysis. In another article [26], he extended Bödewadt flow problem for the case where disk was assumed circumferentially in radial direction with uniform rate. Mustafa et al. [27] extended this problem for nanofluid comprising five different kinds of nanoparticles. Recent contributions in this direction include this [28-33].

Homogeneous heterogeneous reactions are the class of chemical reactions in which reactants occur in single or multi-phase. Chaudhary and Merkin [34] discussed the fluid flow over a flat plate with streamwise pressure gradient within which an isothermal cubic autocatalytic reaction was assumed while single, first order isothermal reaction was considered at the surface. Merkin [35] considered the same model of homogeneous-heterogeneous reaction in a boundary layer flow over a flat plate as in [34]. His findings demonstrate that heterogeneous reaction is dominant near the leading edge of the plate. Bachok et al. [36] observed the behaviors of

2

homogeneous-heterogeneous reaction in stagnation point flow near a deforming sheet. Shaw et al. [37] studied the effects of homogeneous-heterogeneous reactions in micropolar fluid flow over a permeable surface immersed in a porous space. Later kameswaran et al. [38] discussed nanofluid flow near a porous surface inspired byhomogeneous-heterogeneous reactions. Hayat et al. [39] provided analytical treatment for three-dimensional Maxwell fluid flow withhomogeneous-heterogeneous reactions. Few recent papers in this domain are published by Hayat et al. [40, 41], Ramzan et al. [42] and Radiah et al. [43].

The thesis aims to explore Maxwell fluid flow in a rotating frame with heat and mass transfer aspects. Chapter 2 presents a detailed review of an article by Mustafa et al. [33] which deals with the rotating flow of viscoelastic fluid bounded by an exponentially deforming sheet. Chapter 3presents the modeling of homogeneous-heterogeneous reaction effects for flow past a linearly stretching sheet in rotating Maxwell fluid. Numerical results have been derived by a convenient shooting approach and the behaviors of parameters on the solutions are elucidated by plotting graphs. The computations are also developed by MATLAB built in routine bvp4c. In addition, the solutions are compared with the previously published articles in a limiting case and such comparison appears convincing.

1.2   Basic definitions

1.2.1Newtonian fluids

Newtonian fluids are those fluids which fulfill the Newton's law of viscosity.Newton's law of viscosity is given by

$$\tau_{xy} = \mu \frac{du}{dy}, \qquad (1.1)$$

where$\tau$is shear stress, μ is the viscosity of the fluid known as dynamic viscosity and $du/dy$is the shear rate or rate of strain.In these fluids, the graph between stress and shear rate is a straight line. Commonexamples are water, air and milk etc.

1.2.2 Non-Newtonian fluids

Non-Newtonian fluids are those fluids in which shear stress is non-linearly proportional to the shear rate. For many non-Newtonian fluids, the shear stress τ_{xy} is related to the deformation rate by the power law model. Mathematically,

$$\tau_{xy} = k \left(\frac{du}{dy}\right)^n,$$

(1.2)

where k stands for consistency index and n denotes the flow behavior index.

Eq. (1.2) can be written in the following form:

$$\tau_{xy} = \eta \left(\frac{du}{dy}\right),$$

(1.3)

in which $\eta = k \left(\frac{du}{dy}\right)^{n-1}$ represents the apparent viscosity. When $n < 1$, Eq. (1.3) represents shear-thinning (pseudoplastic) fluids while Eq. (1.3) indicates shear-thickening (dialtant) fluids for $n > 1$.
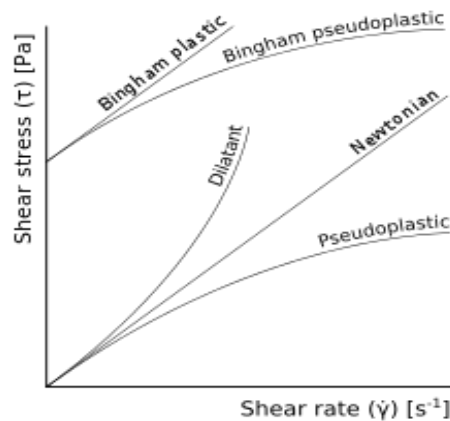

Fig. 1.1: Non-Newtonian fluid

1.2.3 Compressible and incompressible flows

Fluid flow is said to be compressible if fluid density changes with its pressure and Mach number is greater than 0.3. Gasses are generally treated as compressible fluids.

Whereas, a fluid flow is said to be incompressible if fluid density remains constant everywhere or Mach number is less than 0.3. Liquids are often considered as incompressible fluids.

1.2.4 Steady and unsteady flows

A flow in which pressure, velocity, temperature and other properties of the fluid are independent of time at any point in the flow field is called a steady flow. Mathematically speaking,

$$\frac{\partial P}{\partial t} = 0, \tag{1.4}$$

where $P(x, y, z)$ is any property like pressure, velocity, density etc.

An unsteady flow is the one in which fluid properties change with the variation in time at any given point in the flow field.

1.2.5 Laminar and turbulent flows

A fluid flow is called laminar if the fluid particles move in parallel layers and this type of flow occurs typically with low Reynolds number.

Turbulent flow is a type of fluid flow in which particles of fluid fluctuate randomly or mixing and this type of flow occurs typically with higher Reynolds number.

1.2.6 Boundary layer

Boundary layer refers to a thin layer of viscous fluid close to the boundary. As the fluid particles adhere to the wall of surface at rest, the velocity of fluid increases from zero at the surface to the free stream velocity U_e outside the boundary layer. Boundary layer is classified as either laminar or turbulent depending on the value of Reynolds number.
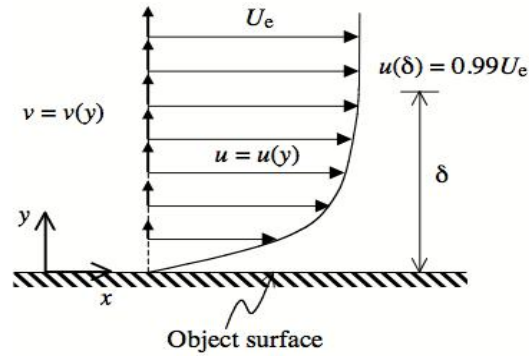
Fig. 1.2: Boundary layer thickness for fluid flow past a stationary plate.

1.2.7 Chemical reaction

Chemical reaction is a process of rearrangement of same or different elements to form a new element or substance. While they do so, they either absorb heat or release heat energy. Reactions occur when more than two molecules interact with each other and the molecules change.New molecules are formed by the change of bonds between atoms.

1.2.8 Homogeneous-heterogeneous reactions

When reactants and products are in the same phase the chemical reaction is defined as homogeneous reaction while, the chemical reaction in which reactants are in two or more phases are known as heterogeneous reaction. Reactions that take place on the surface of a catalyst are also heterogeneous.

1.2.9 Deborah number

The ratio offluid relaxation time t_c to the fluid characteristic time t_p is referred as Deborah number (De). Mathematically,

$$De = \frac{t_c}{t_p}. \tag{1.5}$$

At low Deborah number $D_e \ll 1$, the material displays fluid-like behavior while at higher Deborah number $De \gg 1$, the material demonstrates solid-like behavior.

1.2.10 Schmidt number

The ratio of momentum diffusivity (ν) and the mass diffusivity (D) is referred as Schmidt number (Sc). Mathematically, it is expressed as

$$Sc = \frac{\nu}{D}. \tag{1.6}$$

Thus Schmidt number relates the thickness of hydrodynamic boundary layer with the concentration boundary layer thickness.

1.3 Boundary layer Equation for rotating flow of Maxwell fluid

The equations describing the incompressible flow of Maxwell fluid in rotating frame are as under:

$$\nabla \cdot \mathbf{V} = 0, \tag{1.7}$$

$$\rho \left[\frac{d\mathbf{V}}{dt} + 2\mathbf{\Omega} \times \mathbf{V} + \mathbf{\Omega} \times (\mathbf{\Omega} \times \mathbf{r}) \right] = -\nabla p + \nabla \cdot \mathbf{S}, \tag{1.8}$$

where $\mathbf{V} = \big(u(x,y,z), v(x,y,z), w(x,y,z)\big)$ is the velocity vector, ρ the fluid density, $\frac{d}{dt}$ is the material derivative, $\mathbf{\Omega} = [0,0,\Omega]$ the angular velocity, $\mathbf{r}$ is the radius vector, $\mathbf{S}$ is the extra stress tensor respectively.

In component form, Eq. (1.7) can be expressed as

$$\frac{\partial u}{\partial x} + \frac{\partial v}{\partial y} + \frac{\partial w}{\partial z} = 0. \tag{1.9}$$

For Maxwell fluid, the extra stress tensor obeys the following relationship:

$$\mathbf{S} + \lambda_1 \frac{D\mathbf{S}}{Dt} = \mu \mathbf{A_1}, \tag{1.10}$$

where λ_1 is the fluid relaxation time, D/Dt is the convected time derivative and $\mathbf{A_1}$ is the first Rivlin-Erickson tensor defined as:

$$\mathbf{A_1} = (\nabla \mathbf{V}) + (\nabla \mathbf{V})^t = \begin{bmatrix} 2\,u_x & u_y + v_x & u_z + w_x \\ u_y + v_x & 2v_y & v_z + w_y \\ w_x + u_z & w_y + v_z & 2w_z \end{bmatrix}. \tag{1.11}$$

For any vector $\mathbf{A}$, the upper-convected derivative D/Dt is defined as

$$\frac{D\mathbf{A}_i}{Dt} = \frac{\partial \mathbf{A}_i}{\partial t} + V_j \mathbf{A}_{i,j} - V_{i,j}\mathbf{A}_j, \tag{1.12}$$

By taking $\mathbf{r} = (x, y, z)$ and $\mathbf{\Omega} = (0,0,\Omega)$, centrifugal force term can be expressed as

$$\mathbf{\Omega} \times (\mathbf{\Omega} \times \mathbf{r}) = -\nabla \left(\frac{\Omega^2 r^2}{2} \right). \tag{1.13}$$

Using Eq. (1.13) in Eq. (1.8), one obtains

$$\rho \left[\frac{d\mathbf{V}}{dt} + 2\mathbf{\Omega} \times \mathbf{V} \right] = -\nabla p^* + \nabla.\mathbf{S}, \tag{1.14}$$

where $p^* = p - \rho \frac{\Omega^2 r^2}{2}$ is the modified pressure.

Now assigning the operator $\left(1 + \lambda_1 \frac{D}{Dt} \right)$ on both sides of Eq. (1.14), we have

$$\rho \left(1 + \lambda_1 \frac{D}{Dt} \right) \left[\frac{d\mathbf{V}}{dt} + 2\mathbf{\Omega} \times \mathbf{V} \right] = -\left(1 + \lambda_1 \frac{D}{Dt} \right) \nabla p^* + \left(1 + \lambda_1 \frac{D}{Dt} \right)(\nabla.\mathbf{S}). \tag{1.15}$$

Assuming that there is no modified pressure gradient we have

$$\rho\left(1 + \lambda_1 \frac{D}{Dt}\right)\left[\frac{d\mathbf{V}}{dt} + 2\mathbf{\Omega} \times \mathbf{V}\right] = \nabla.\left(1 + \lambda_1 \frac{D}{Dt}\right)\mathbf{S}. \tag{1.16}$$

Making use of Eq. (1.10), Eq. (1.16) can be expressed as

$$\rho\left[\left(1 + \lambda_1 \frac{D}{Dt}\right)\left(\frac{d\mathbf{V}}{dt}\right) + \left(1 + \lambda_1 \frac{D}{Dt}\right)(2\mathbf{\Omega} \times \mathbf{V})\right] = \mu(\nabla.\mathbf{A_1}). \tag{1.17}$$

Using definitions (1.11) and (1.12), the $x-$ and $y-$ components of (1.17) can be obtained in the following forms:

$$u\frac{\partial u}{\partial x} + v\frac{\partial u}{\partial y} + w\frac{\partial u}{\partial z} - 2\Omega v + \lambda_1 \left\{ \begin{array}{c} u^2\frac{\partial^2 u}{\partial x^2} + v^2\frac{\partial^2 u}{\partial y^2} + w^2\frac{\partial^2 u}{\partial z^2} \\ +2uv\frac{\partial^2 u}{\partial x \partial y} + 2vw\frac{\partial^2 u}{\partial y \partial z} + 2uw\frac{\partial^2 u}{\partial x \partial z} \\ -2\Omega\left(u\frac{\partial v}{\partial x} + v\frac{\partial v}{\partial y} + w\frac{\partial v}{\partial z}\right) + 2\Omega\left(v\frac{\partial u}{\partial x} - u\frac{\partial u}{\partial y}\right) \end{array} \right\} = v\frac{\partial^2 u}{\partial z^2}, \tag{1.18}$$

$$u\frac{\partial v}{\partial x} + v\frac{\partial v}{\partial y} + w\frac{\partial v}{\partial z} + 2\Omega u + \lambda_1 \left\{ \begin{array}{c} u^2\frac{\partial^2 v}{\partial x^2} + v^2\frac{\partial^2 v}{\partial y^2} + w^2\frac{\partial^2 v}{\partial z^2} \\ +2uv\frac{\partial^2 v}{\partial x \partial y} + 2vw\frac{\partial^2 v}{\partial y \partial z} + 2uw\frac{\partial^2 v}{\partial x \partial z} \\ +2\Omega\left(u\frac{\partial u}{\partial x} + v\frac{\partial u}{\partial y} + w\frac{\partial u}{\partial z}\right) + 2\Omega\left(v\frac{\partial v}{\partial x} - u\frac{\partial v}{\partial y}\right) \end{array} \right\} = v\frac{\partial^2 v}{\partial z^2}. \tag{1.19}$$

1.4 Equation of heat transfer

The heat transfer phenomenon describes the transfer of thermal energy from hotter body to cooler body. The relevant equation describing the heat transfer effect in the presence of radiation is:

$$\rho c_p \frac{dT}{dt} = K\nabla^2 T - \frac{\partial q_r}{\partial z}, \tag{1.20}$$

where ρ is the density, c_p denotes the specific heat capacity, T represents the local temperature and q_r denotes the radiation heat flux given by Rosseland [44] as

$$q_r = -\frac{4}{3}\frac{a_R}{k^*}\frac{\partial T^4}{\partial z},$$

in which a_R represents the Stefan Boltzmann constant and k^* stands for mean absorption coefficient.

Applying boundary layer assumptions, Eq. (1.20) yields:

$$u\frac{\partial T}{\partial x} + v\frac{\partial T}{\partial y} + w\frac{\partial T}{\partial z} = \alpha\frac{\partial^2 T}{\partial z^2} - \frac{1}{(\rho c_p)}\frac{\partial q_r}{\partial z}, \tag{1.21}$$

1.5 Equation of mass transfer

The relevant equations describing the diffusion process under homogeneous-heterogeneous reaction are [34]

$$\mathbf{V}.\nabla a = \nabla.D_A\nabla a - k_c ab^2, \tag{1.22}$$

$$\mathbf{V}.\nabla b = \nabla.D_B\nabla b + k_c ab^2, \tag{1.23}$$

where D_A and D_B stand for diffusion coefficients for reactants A and B respectively and the last terms of (1.22) and (1.23) indicate the consumption rate of chemical specie A and product rate of chemical species B respectively.

Employing boundary layer assumptions, (1.22) and (1.23) can be simplified to yield the following:

$$u\frac{\partial a}{\partial x} + v\frac{\partial a}{\partial y} + w\frac{\partial a}{\partial z} = D_A\frac{\partial^2 a}{\partial z^2} - k_c ab^2, \tag{1.24}$$

$$u\frac{\partial b}{\partial x} + v\frac{\partial b}{\partial y} + w\frac{\partial b}{\partial z} = D_B\frac{\partial^2 b}{\partial z^2} + k_c ab^2. \tag{1.25}$$

Chapter 2

Rotating flow of Maxwell fluid over an exponentially stretching surface with non-linear radiative heat transfer

This chapter includes a detailed review of a recent article by Mustafa et al. [33] which deals with the rotating flow of viscoelastic fluid over an exponentially stretching surface. Effect of non-linear radiative heat flux on thermal boundary layer is considered. A set of transformations are applied to non-dimensionalize the resulting boundary layer equations. Shooting approach, based on fifth-order Runge-kutta integration, is implemented to present numerical computations. We observe that rotation and viscoelasticity decrease the hydrodynamic boundary layer thickness. For sufficiently large value of θ_w, temperature function has an interesting S shaped profile. Heat transfer rate decreases for increasing values of rotation parameter Ω.

2.1 Problem formulation

Consider a steady flow of an incompressible Maxwell fluid over a surface which is stretched exponentially in the x-direction with the velocity $u_w = u_0 \exp(x/L)$, where u_0 represents reference velocity and L denotes characteristics length. The fluid occupies semi-infinite domain $z \geq 0$. Fluid rotates around z-axis with constant angular velocity $\bar{\Omega}$. The function $T_w(x) = T_\infty + T_0 \exp(Ax/2L)$ prescribes the wall temperature in which T_0 and T_∞ are reference and ambient temperatures respectively. The conservation relations of mass, momentum and energy can be cast into the following form (see Mustafa et al. [33] for details):

$$\frac{\partial u}{\partial x} + \frac{\partial v}{\partial y} + \frac{\partial w}{\partial z} = 0, \tag{2.1}$$

$$u\frac{\partial u}{\partial x} + v\frac{\partial u}{\partial y} + w\frac{\partial u}{\partial z} - 2\bar{\Omega}v + \lambda_1 \begin{cases} u^2\frac{\partial^2 u}{\partial x^2} + v^2\frac{\partial^2 u}{\partial y^2} + w^2\frac{\partial^2 u}{\partial z^2} \\ +2uv\frac{\partial^2 u}{\partial x\partial y} + 2vw\frac{\partial^2 u}{\partial y\partial z} + 2uw\frac{\partial^2 u}{\partial x\partial z} \\ -2\bar{\Omega}\left(u\frac{\partial v}{\partial x} + v\frac{\partial v}{\partial y} + w\frac{\partial v}{\partial z}\right) + 2\bar{\Omega}\left(v\frac{\partial u}{\partial x} - u\frac{\partial u}{\partial y}\right) \end{cases} = v\frac{\partial^2 u}{\partial z^2}, \tag{2.2}$$

$$u\frac{\partial v}{\partial x} + v\frac{\partial v}{\partial y} + w\frac{\partial v}{\partial z} + 2\bar{\Omega}u + \lambda_1 \begin{cases} u^2\frac{\partial^2 v}{\partial x^2} + v^2\frac{\partial^2 v}{\partial y^2} + w^2\frac{\partial^2 v}{\partial z^2} \\ +2uv\frac{\partial^2 v}{\partial x\partial y} + 2vw\frac{\partial^2 v}{\partial y\partial z} + 2uw\frac{\partial^2 v}{\partial x\partial z} \\ +2\bar{\Omega}\left(u\frac{\partial u}{\partial x} + v\frac{\partial u}{\partial y} + w\frac{\partial u}{\partial z}\right) + 2\bar{\Omega}\left(v\frac{\partial v}{\partial x} - u\frac{\partial v}{\partial y}\right) \end{cases} = v\frac{\partial^2 v}{\partial z^2}, \tag{2.3}$$

$$u\frac{\partial T}{\partial x} + v\frac{\partial T}{\partial y} + w\frac{\partial T}{\partial z} = \alpha\frac{\partial^2 T}{\partial z^2} - \frac{1}{(\rho c_p)}\frac{\partial q_r}{\partial z}, \tag{2.4}$$

where u, v and w denote the velocity components along the x, y and $z-$ directions respectively, λ_1 is the fluid relaxation time, v the kinematic viscosity, ρ is the fluid density, c_p the specific heat capacity, T the local temperature, α the thermal diffusivity and q_r denotes the radiation heat flux given by Rosseland [44] as

$$q_r = -\frac{4}{3}\frac{a_R}{k^*}\frac{\partial T^4}{\partial z},$$

in which a_R represents the Stefan Boltzmann constant and k^* stands for mean absorption coefficient. The prescribed conditions are:

$$u = u_w(x) = u_0\,exp\left(\frac{x}{L}\right), \quad v = 0, \quad w = 0, \qquad T = T_w(x) = T_0\,exp\left(\frac{Ax}{2L}\right) + T_\infty \quad at \ z = 0,$$

$$u \to 0, \qquad v \to 0, \qquad T \to T_\infty \qquad as \quad z \to \infty. \tag{2.5}$$

Consider the following set of transformations [9]

$$\eta = z\sqrt{\frac{u_0}{2vL}}\,exp\left(\frac{x}{2L}\right), \quad u = u_0 exp\left(\frac{x}{L}\right)f'(\eta), \quad v = u_0 exp\left(\frac{x}{L}\right)g(\eta),$$

$$w = -\sqrt{\frac{vu_0}{2L}}\,exp\left(\frac{x}{2L}\right)[f + \eta f'], \qquad \theta(\eta) = \frac{T - T_\infty}{T_w - T_\infty}. \tag{2.6}$$

Eq. (2.1) is satisfied identically whereas Eqs. (2.2) - (2.5) change into the following form

$$f''' - 2f'^2 + ff'' - \frac{\gamma}{2}\left(4f'^3 - \eta f'^2 f'' + f^2 f''' - 6ff'f''\right) + \tag{2.7}$$

$$\Omega[4g - 2\gamma(g'f + \eta f''g)] = 0,$$

$$g'' - 2f'g + fg' - \frac{\gamma}{2}\left(4f'^2 g - \eta f'^2 g' + f^2 g'' - 6ff'g' + 4\Omega[-f' \tag{2.8}\right.$$

$$+ \gamma\left(-f'^2 - g^2 - \frac{\eta}{2}gg' + \frac{1}{2}ff''\right) = 0,$$

$$\frac{1}{Pr}[(1 + Rd(1 + (\theta_w - 1)\theta)^3)\theta']' + f\theta' - Af'\theta = 0, \tag{2.9}$$

$$f(0) = 0, \quad g(0) = 0, \qquad f'(0) = 1, \qquad \theta(0) = 1,$$

$$f'(+\infty) \to 0, \quad g(+\infty) \to 0, \quad \theta(+\infty) \to 0 \tag{2.10}$$

where $\Omega = L\bar{\Omega}/u_w$ is the local rotation parameter, $\gamma = \lambda_1 u_w/L$ denotes thelocal Deborah number, $Pr = v/\alpha$ is the Prandtl number, $\theta_w = T_w/T_\infty$ is the temperature ratio parameter and $Rd = 16a_R T_\infty^3/3k^* k$ is the radiation parameter.

$$Nu_x = \frac{xq_w}{k(T_w - T_\infty)}, \tag{2.11}$$

where $q_w = -k\left(\frac{\partial T}{\partial z}\right)_{z=0}$ is a wall heat flux. Through transformations (2.6), Eq. (2.11) can be expressed as below:

$$\frac{L}{x}\sqrt{\frac{2}{Re_x}}Nu_x = -(1 + Rd\theta_w^3)\theta'(0), \tag{2.12}$$

where $Re_x = u_w L/v$ represents the local Reynold's number.

2.2 Numerical technique

The numerical solution of differential Eqs. (2.7) - (2.9) along with the boundary condition (2.10) is obtainedvia shooting approach. Converting Eqs. (2.7) – (2.9) into a system of first-order equations by the following substitutions:

$$y_1 = f, \ y_2 = f', \ y_3 = f'', y_4 = g, \ y_5 = g', \ y_6 = \theta, \ y_7 = \theta',$$

we get the following

$$
\begin{bmatrix} y_1' \\ y_2' y_3 \\ y_3' \\ y_4' \\ y_5' \\ y_6' y_7 \\ y_7' \end{bmatrix} =
\begin{bmatrix} y_2 \\ y_3 \\ \dfrac{2y_2^2 + y_1 y_3 - \Omega[4y_4 - 2\gamma(y_1 y_5 + \eta y_3 y_4)] + 0.5\gamma(4y_2^3 - \eta y_2^2 y_3 - 6y_1 y_2 y_3)}{1 - (0.5)\gamma y_1^2} \\ y_5 \\ \dfrac{2y_2 y_4 - y_1 y_5 - 4\Omega[-y_2 + \gamma(-y_2^2 - y_4^2 - (0.5)\eta y_4 y_5 + (0.5)y_1 y_3] + (0.5)\gamma(4y_2^2 y_4 - \eta y_2^2 y_5 - 6y_1 y_2 y_5)}{1 - (0.5)\gamma y_1^2} \\ y_7 \\ \dfrac{-3Rd(1 + (\theta_w - 1)y_6)^2(\theta_w - 1)y_7^2 + \Pr(Ay_2 y_6 - y_1 y_7)}{1 + Rd(1 + (\theta_w - 1)y_6)^3} \end{bmatrix} ,
$$

(2.13)

and the initial conditions are:

$$
\begin{bmatrix} y_1(0) \\ y_2(0) \\ y_3(0) \\ y_4(0) \\ y_5(0) \\ y_6(0) \\ y_7(0) \end{bmatrix} =
\begin{bmatrix} 0 \\ 1 \\ t \\ 0 \\ s \\ 1 \\ v \end{bmatrix},
$$

(2.14)

First-order equations have been integrated viafifth-order Runge-Kutta approach. Newton's method is used to estimate the values of unknown slopes with the appropriate guesses by taking $f''(0) = t, \quad g'(0) = s, \quad \theta'(0) = v$ until the boundary conditions at infinity are satisfied. All computations have been done in MATLAB.
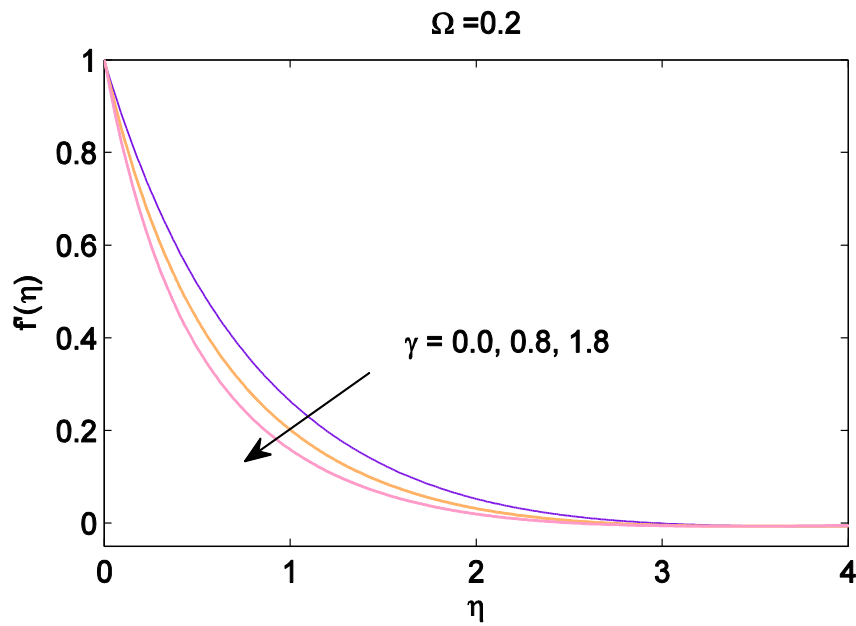
2.3 Results and discussion

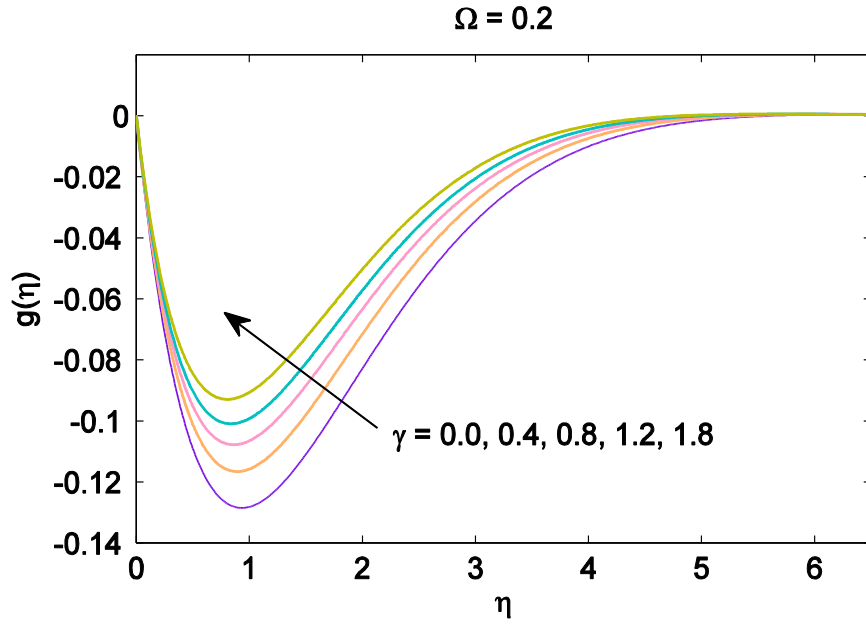Fig. 2.1: Profile of f' for different values of γ.
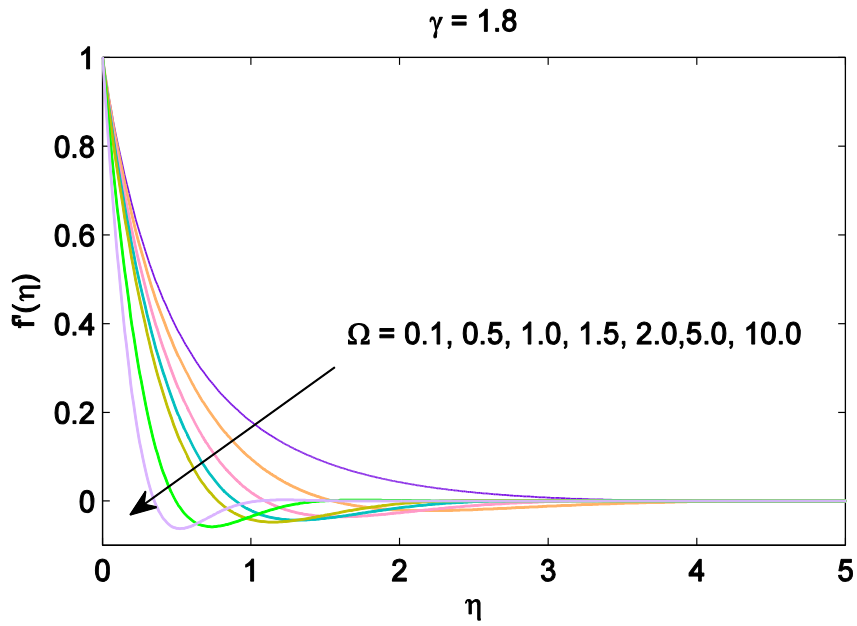
Fig. 2.2: Profile of g for different values of γ.

Fig. 2.3: Profile of f' for different values of Ω.
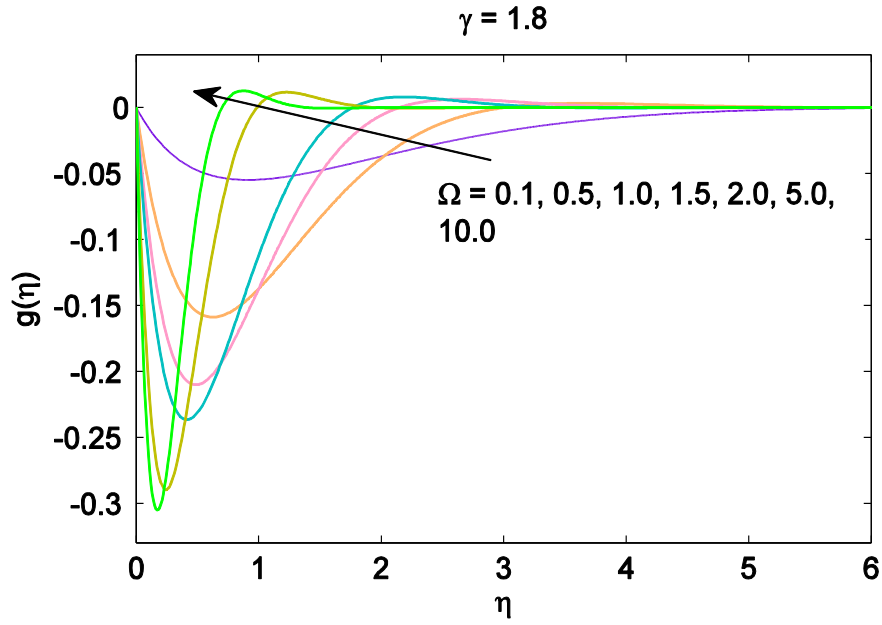
Fig. 2.4: Profile of *g* for different values of Ω.
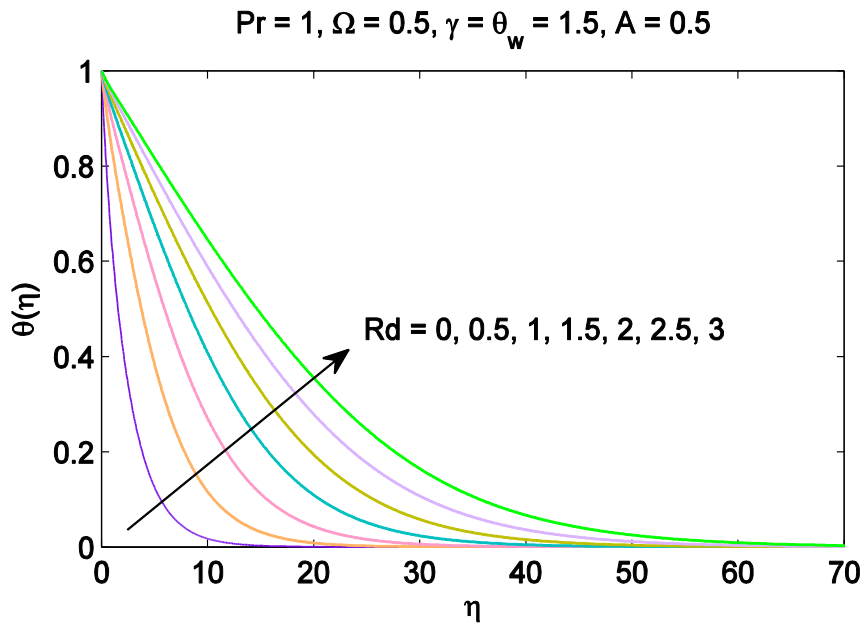
Fig. 2.5: Profile of θ for different values of Rd.
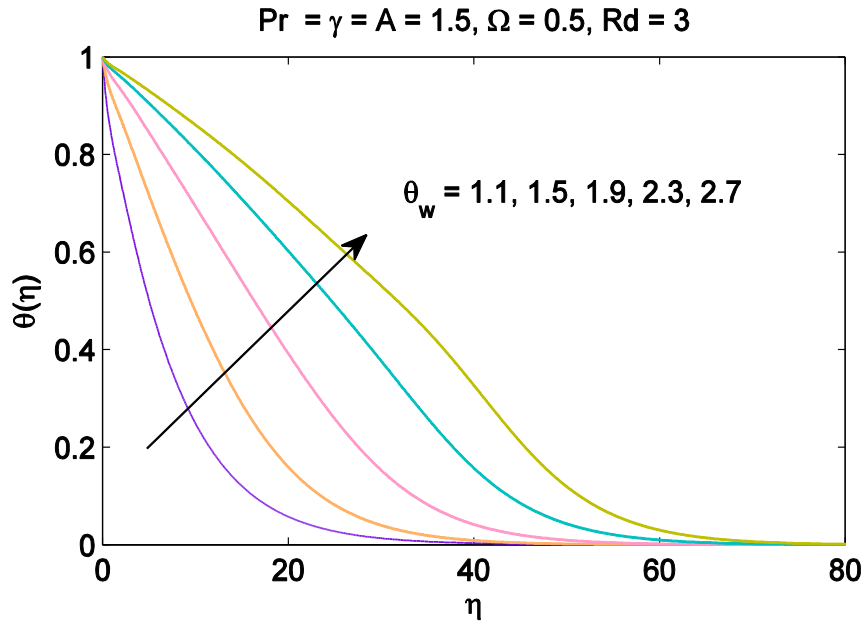
Fig. 2.6: Profile of θ for different values of θ_w.
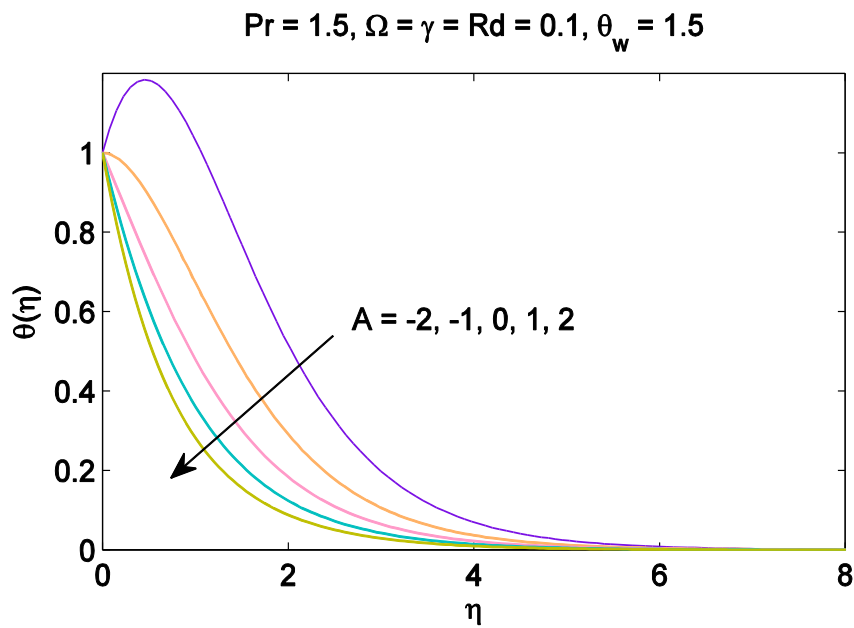
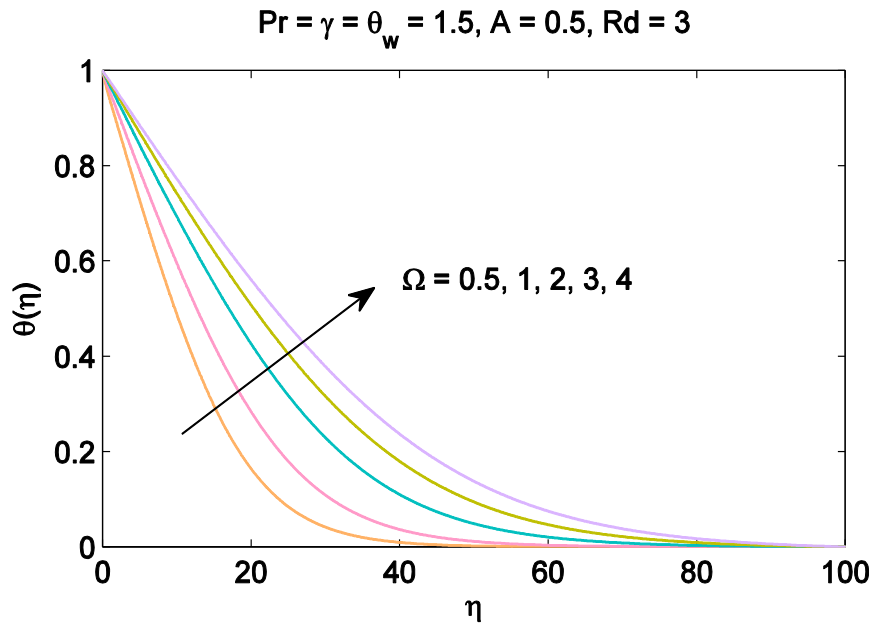Fig. 2.7: Profile of θ for different values of A.

18

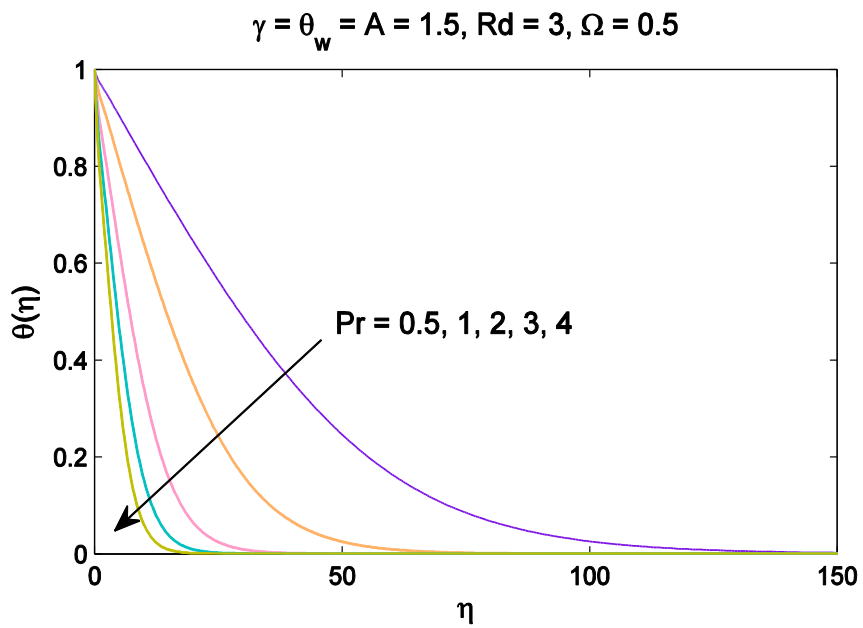Fig. 2.8: Profile of θ for different values of Ω.

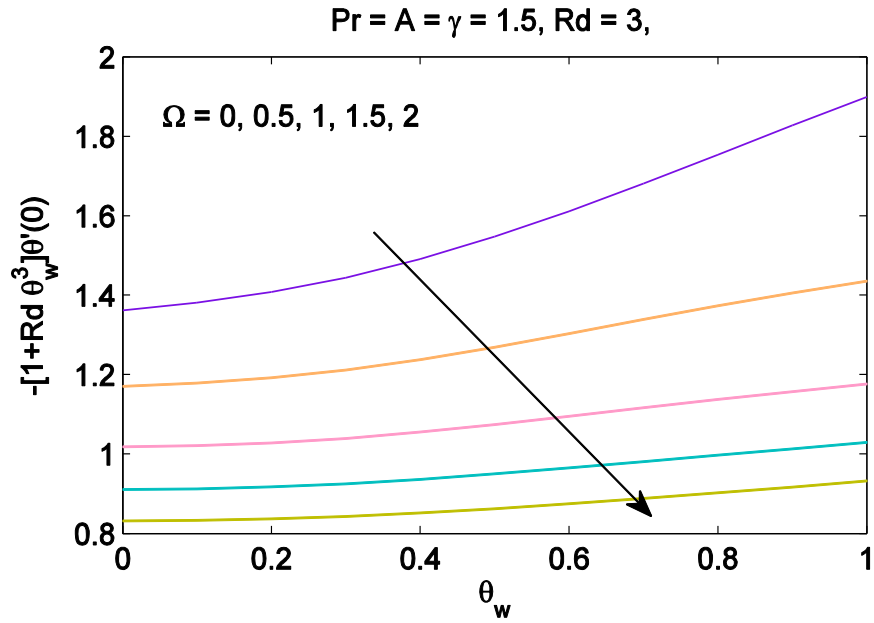Fig. 2.9: Profile of θ for different values of Pr.

Fig. 2.10: Profile of $-(1 + Rd\theta_w^3)\theta'(0)$ for different values of Ω.
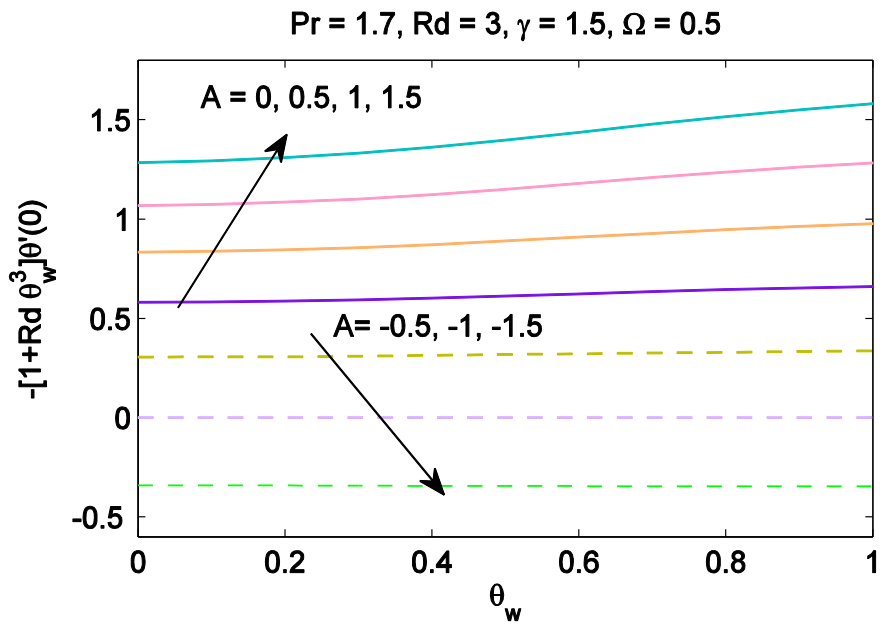

Fig. 2.11: Profile of $-(1 + Rd\theta_w^3)\theta'(0)$ for different values of A.

Table 2.1: Comparison of computational results of $-f''(0)$ and $-g'(0)$ with those of Javed et al. [23] at $\gamma = 0$.

Ω	$-f''(0)$		$-g'(0)$	
	Javed et al.[23]	Present results	Javed et al. [23]	Present results
0.2	1.3474169	1.3474204	0.37015223	0.3701525
0.5	1.5194131	1.5194195	0.76251409	0.7625143
2	2.2827966	2.2828127	1.8485044	1.8485032
5	3.3444338	3.3444606	3.0609192	3.0609164
10	4.6017220	4.6017610	4.3990640	4.3990580
50	10.058172	10.058260	9.9668099	9.9667990
100	14.183223	14.183358	14.118628	14.118612

Table 2.2: Numerical values of local Nusselt number $-(1 + Rd\theta_\infty^3)\theta'(0)$ for various values of $Pr, Rd, \Omega, \theta_w, A$ and γ.

Pr	Rd	Ω	θ_w	A	γ	$-(1 + Rd\theta_w^3)\theta'(0)$
0.5	1	0.5	1.5	0.5	1.5	0.1824399
1						0.3683380
1.5						0.5597549
3						1.1557117
	0					0.5585281
	1					0.5597549
	2					0.5599698
	3					0.5610885
		0				1.4881180
		1.5				0.2510547
		3				0.1914879
		4.5				0.1678869
			1.5			0.5599698
			2.5			1.1227470
			3.5			3.3188390
			4.5			17.324120
1.5	2	0.5	1.5	-2		-0.3619706
				-1		0.0122859
				0		0.3792183
				1		0.7389305
				2		1.0915300
				1.5	0	1.7411790
					0.6	1.3768130
					1.2	1.0589910
					1.8	0.7372889

The validity of present numerical scheme is established by comparing the numerical results of $-f''(0)$ and $-g'(0)$ with those of [23]. The results are found in complete agreement for full range of rotation-strength parameter λ (see table 2.1).Table 2.2 gives the computational results of heat transfer coefficient $-(1 + Rd\theta_\infty^3)\theta'(0)$ for various parameter values. It is apparent that heat transfer improves as the value of Pr, Rd, θ_w and A is increased. On the other hand, magnitude of local Nusselt number is inversely proportional to both fluid relaxation time and rotation rateΩ.

Fig 2.1 demonstrates the influence of local Deborah number on the velocity profile f'. Deborah number is the ratio of relaxation time to the characteristic time.For larger value of γ, the relaxation time is large as compared to the observation time scale and materials response is solid like. That's why fluid flow in $x-$ direction is resisted by increasing Deborah number. Consequently, velocity profile f' decreases and boundary layer becomes thinner whenγ is increased.

Fig. 2.2 demonstrates the change in velocity profile $g(\eta)$ as local Deborah number γ is incresaed. The value of $g(\eta)$ is negative illustrating that fluid flow towards negative $y-$direction due to counterclockwise rotation.

Figures 2.3 and 2.4 portray the behavior of rotation parameter Ω on the velocity profile f' and g respectively.Fig. 2.3 illustrates thatf' is negative in the vicinity of the surface when$\Omega = 10$. For smaller values ofΩ the decrease in f' with η is monotonic. When Ω is large, there is some oscillation in the velocity profiles which is attributed to the rotating frame. In fact, the decay in f' with η is oscillatory when larger Ω is chosen. Boundary layer thickness is also inversely proportional toΩ.

Fig. 2.5 shows the profile of temperature θ for different values of radiation parameterRd. It can be seen that temperature profile enhances by the increase of radiation parameterRd.

Fig. 2.6 is prepared to examine the influence of $\theta_w$on temperature profile θ. It should be noted that $\theta'(0)$ approaches zero as θ_w is increased and this is signaled by the S-shaped curves of temperature $\theta(\eta)$ when lager values of θ_w are considered.

In Fig. 2.7, we present the change in temperature $\theta(\eta)$ with the variation in temperature exponent parameter A. Temperature θ decreases when parameter A is increased. It can be seen

that temperature θ rises for the first value of parameter A and then velocity profile moves towards the stretching sheet when $A = -1$. In literature, this effect is known as "Sparrow-Gregg type Hill (SGH)", phenomenon.

Fig. 2.8 analyzes the behavior of rotation-strength parameterΩ on temperature profile. As rotational parameter is incremented then the temperature rises and its profile become thicker.

Fig. 2.9 shows the change in $\theta(\eta)$ whenPrandtl number Pr is varied.Prandtl number compares the thickness of thermal and hydrodynamic boundary layers. Since Pr has inverse relationship with thermal diffusivity. Thus a larger Prandtl number implies lower thermal diffusivity and shorter penetration depth. However, the slope of $\theta(\eta)$ near the stretching sheet is larger for higher Prandtl number.

Fig. 2.10 exhibits the influence of temperature ratio parameterθ_w and rotation parameterΩ on the heat transfer coefficient $-(1 + Rd\theta_w^3)\theta'(0)$. Local Nusselt number increases nonlinearly when θ_w is incremented. When θ_w gradually enlarges, it results in growth in wall temperature and consequently, growth in heat transfer rate. Heat transfer rate also improves when fluid rotates at a higher rate.

Fig. 2.11 presents the impact of A and θ_w on the heat transfer coefficient $-(1 + Rd\theta_w^3)\theta'(0)$. Magnitude of $-(1 + Rd\theta_w^3)\theta'(0)$rises when values of A are incremented. This shows that parameter A enhance the heat transfer rate from the surface. However, some negative values of A corresponds the negative Nusselt number.

Chapter 3

Effects of homogeneous-heterogeneous reactions on rotating flow of Maxwell fluid due to linearly stretching sheet

This study provides numerical treatment for rotating flow of Maxwell fluid which occurs due to deformation of plane surface. Mass transfer analysis is carried out in the existence of homogeneous-heterogeneous reactions. By means of usual transformation, the governing equations are changed into global similarity equations. Velocity and concentration profiles are computed for broad range of viscoelastic fluid parameter. The solutions contain a rotation strength parameter λ that has considerable effect on the flow field. For sufficiently large value of λ, the velocity fields are oscillatory decaying function of the non-dimensional vertical distance. Solute concentration at the surface is found to decrease upon increasing strengths of chemical reactions. A comparative study of present computations with those of already published ones appears convincing.

3.1 Introduction

In this chapter, consider a laminar flow of binary viscoelastic fluid obeying Maxwell model due to stretching of a plane elastic surface. We select a Cartesian coordinate frame in which $z-$ axis is aligned vertically upward and surface occupies the $xy-$ plane. Maxwell fluid filling half space $z > 0$ rotates uniformly about $z-$ axis with rate Ω. Further we consider the presence of chemically reacting species in the flow field. The existence of coriolis force makes the problem three-dimensional. We take into account the homogeneous-heterogeneous reactions model proposed by Chaudhary and Merkin [34]:

$$A + 2B \rightarrow 3B \quad rate = k_c ab^2, \tag{3.1}$$

while we have a catalyst surface with simple, isothermal and first-order reaction given by

$$A \rightarrow B \quad rate = k_s a, \tag{3.2}$$

where a and b denote the concentration of species A and B while k_c and k_s are constants. The scheme (3.1) ensures that reaction rate at the outer edge of boundary layer is zero.

In usual notations, equations describing the flow of Maxwell fluid with chemically reactive species are:

$$\frac{\partial u}{\partial x} + \frac{\partial v}{\partial y} + \frac{\partial w}{\partial z} = 0, \tag{3.3}$$

$$u\frac{\partial u}{\partial x} + v\frac{\partial u}{\partial y} + w\frac{\partial u}{\partial z} - 2\Omega v + \lambda_1 \left\{ \begin{array}{c} u^2\frac{\partial^2 u}{\partial x^2} + v^2\frac{\partial^2 u}{\partial y^2} + w^2\frac{\partial^2 u}{\partial z^2} \\ +2uv\frac{\partial^2 u}{\partial x\partial y} + 2vw\frac{\partial^2 u}{\partial y\partial z} + 2uw\frac{\partial^2 u}{\partial x\partial z} \\ -2\Omega\left(u\frac{\partial v}{\partial x} + v\frac{\partial v}{\partial y} + w\frac{\partial v}{\partial z}\right) + 2\Omega\left(v\frac{\partial u}{\partial x} - u\frac{\partial u}{\partial y}\right) \end{array} \right\} = v\frac{\partial^2 u}{\partial z^2}, \tag{3.4}$$

$$u\frac{\partial v}{\partial x} + v\frac{\partial v}{\partial y} + w\frac{\partial v}{\partial z} + 2\Omega u + \lambda_1 \left\{ \begin{array}{c} u^2\frac{\partial^2 v}{\partial x^2} + v^2\frac{\partial^2 v}{\partial y^2} + w^2\frac{\partial^2 v}{\partial z^2} \\ +2uv\frac{\partial^2 v}{\partial x\partial y} + 2vw\frac{\partial^2 v}{\partial y\partial z} + 2uw\frac{\partial^2 v}{\partial x\partial z} \\ +2\Omega\left(u\frac{\partial u}{\partial x} + v\frac{\partial u}{\partial y} + w\frac{\partial u}{\partial z}\right) + 2\Omega\left(v\frac{\partial v}{\partial x} - u\frac{\partial v}{\partial y}\right) \end{array} \right\} = v\frac{\partial^2 v}{\partial z^2}, \tag{3.5}$$

$$u\frac{\partial a}{\partial x} + v\frac{\partial a}{\partial y} + w\frac{\partial a}{\partial z} = D_A\frac{\partial^2 a}{\partial z^2} - k_c ab^2, \tag{3.6}$$

$$u\frac{\partial b}{\partial x} + v\frac{\partial b}{\partial y} + w\frac{\partial b}{\partial z} = D_B\frac{\partial^2 b}{\partial z^2} + k_c ab^2. \tag{3.7}$$

The said problem is subjected to following conditions:

$$u = cx, \quad v = 0, \quad w = 0, \quad D_A\frac{\partial a}{\partial z} = k_s a, \quad D_B\frac{\partial b}{\partial z} = -k_s a, \quad at \; z = 0, \tag{3.8}$$

$$u \rightarrow 0, \quad v \rightarrow 0, \quad a \rightarrow a_0, \quad b \rightarrow 0, \quad as \; z \rightarrow \infty. \tag{3.9}$$

Here (u, v, w) denote thevelocitycomponents in the directions of increasing(x, y, z) respectively, λ_1 is the fluid relaxation time, $D_A$and $D_B$stand for diffusion coefficientsfor reactants A and Brespectively, νstands for kinematic viscosity and $c > 0$ denotes the stretch rate. The last term in eq. (3.6) and (3.7) indicate the consumption rate of chemical specie A and product rate of chemical specie B respectively.

Introducing a similarity variable$\eta = \sqrt{\frac{c}{\nu}}z$, we propose the following quantities:

$$u = cxf'(\eta), \quad v = cxg(\eta), \quad w = -\sqrt{c\nu}f(\eta), \quad a = a_0\phi(\eta), \quad b = a_0h(\eta).$$

$$(3.10)$$

The variables (3.10) satisfy the continuity equation (3.1) whereas Eqs. (3.4) – (3.9) transform into the following differential equations:

$$f''' + ff'' - f'^2 + 2\lambda(g - \beta fg') + \beta[2ff'f'' - f^2f'''] = 0, \tag{3.11}$$

$$g'' + fg' - f'g - 2\lambda[f' + \beta(f'^2 - ff'' + g^2)] + \beta[2ff'g' - f^2g''] = 0, \tag{3.12}$$

$$\frac{1}{Sc}\phi'' + f\phi' - K\phi h^2 = 0, \tag{3.13}$$

$$\frac{\delta}{Sc}h'' + fh' + K\phi h^2 = 0, \tag{3.14}$$

$$\text{at } \eta = 0: f = g = 0, \quad f' = 1, \quad \phi' = K_s\phi, \quad \delta h' = -K_s\phi, \tag{3.15}$$

$$\text{as } \eta \to \infty: f' \to 0, \quad g \to 0, \quad \phi \to 1, \quad h \to 0. \tag{3.16}$$

Here $\lambda = \Omega/c$ denotes the rotation-strength parameter, β is the Deborah number, Sc the Schmidt number,δ is the diffusion coefficient,K denotes the homogeneous reactionstrength parameter, and K_s is the (surface) heterogeneous reactionstrength parameter.

$$\beta = \lambda_1 c, \quad Sc = \frac{\nu}{D_A}, \quad K = \frac{k_c a_0^2}{c}, \quad \delta = \frac{D_B}{D_A}, \quad K_s = \frac{k_s}{D_A}\sqrt{\frac{\nu}{c}}. \tag{3.17}$$

In many practical situations, the diffusion coefficients of species a and b are assumed to be of comparable size. This allows us to assume further that the coefficients D_A and D_B are equal, meaning that $\delta \approx 1$. In view of conditions (3.15) and (3.16), we can write

$$\phi(\eta) + h(\eta) = 1, \tag{3.18}$$

whichreduces Eq. (3.13) and (3.14) into following equation:

$$\frac{1}{Sc}\phi'' + f\phi' - K\phi(1-\phi)^2 = 0,$$

(3.19)

subject to the conditions:

$$\phi'(0) = K_s\phi(0) \text{ and } \phi(\infty) \to 1.$$

(3.20)

3.2 Numerical technique

The numerical solution of differential Eq. (3.11), (3.12) and (3.19) along with the boundary condition have been obtained via shooting approach. Converting Eqs. (3.11) – (3.14) into a system of first-order equations by the following substitutions:

$$y_1 = f, \; y_2 = f', \; y_3 = f'', \; y_4 = g, \; y_5 = g', \; y_6 = \phi, \; y_7 = \phi'.$$

We get the following

$$\begin{bmatrix} y_1' \\ y_2' \\ y_3' \\ y_4' \\ y_5' \\ y_6' \\ y_7' \end{bmatrix} = \begin{bmatrix} y_2 \\ y_3 \\ (y_2^2 - y_1y_3 - 2\lambda(y_4 - \beta y_1y_5 - 2\beta y_1y_2y_3)))/(1 - \beta y_1^2) \\ y_5 \\ (y_2y_4 - y_1y_5 + 2\lambda(y_2 + \beta(y_2^2 - y_1y_3 + y_4^2)) - 2\beta y_1y_2y_5)/(1 - \beta y_1^2) \\ y_7 \\ Sc(K\phi(1-\phi)^2 - y_1y_7) \end{bmatrix},$$

(3.21)

and the initial conditions are:

27

$$
\begin{bmatrix}
y_1(0) \\
y_2(0) \\
y_3(0) \\
y_4(0) \\
y_5(0) \\
y_6(0) \\
y_7(0)
\end{bmatrix}
=
\begin{bmatrix}
0 \\
1 \\
t \\
0 \\
s \\
u_3 \\
K_s v
\end{bmatrix}
, \tag{3.22}
$$

First-order equations have been integrated via fifth-order Runge-Kutta approach. Newton's method is used to estimate the values of unknown slopes with the appropriate guesses by taking $f'(0) = t, \quad g(0) = s, \quad \theta(0) = v$ until the boundary conditions at infinity are satisfied. All computations have been done in the MATLAB.
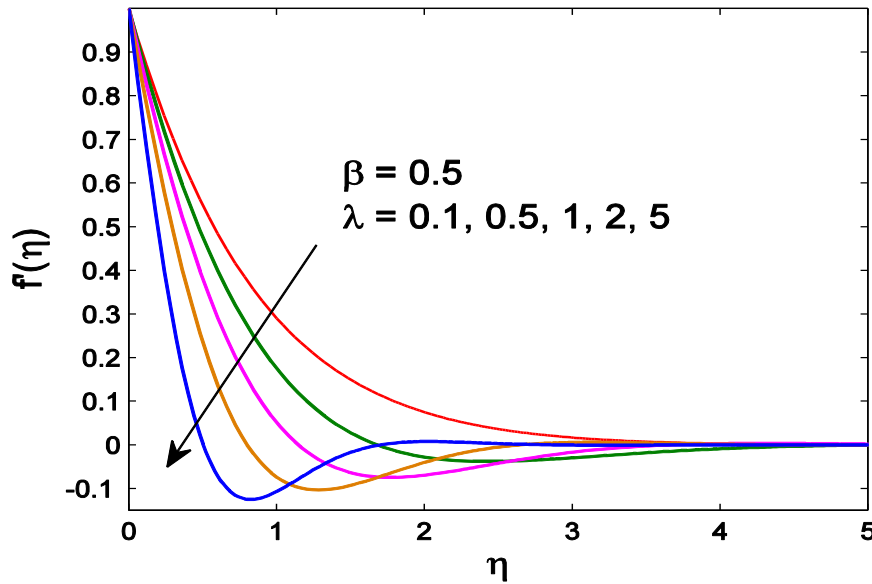
3.3 Results and disscussion

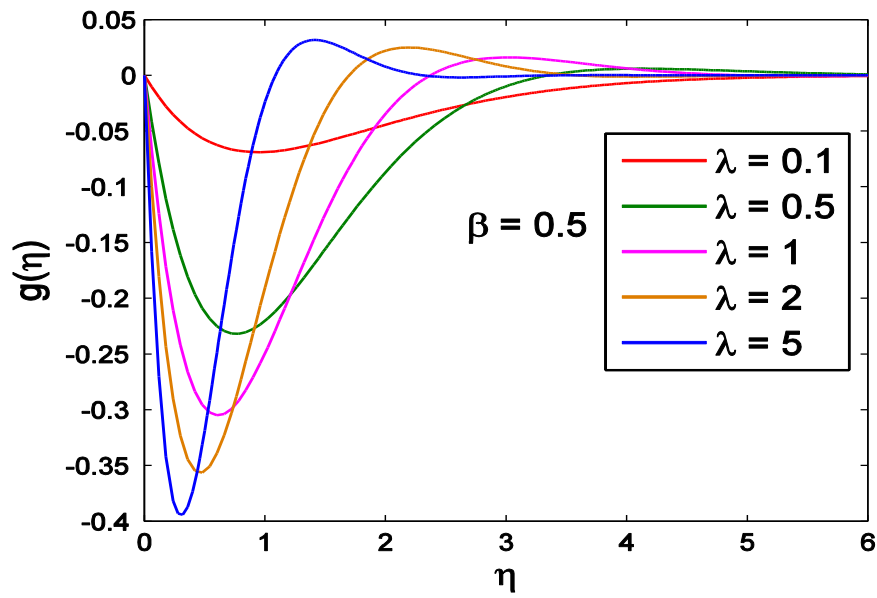Fig. 3.1: Profile of velocity field f' for various values of λ.

Fig. 3.2: Profile of velocity field g for variousvalues of λ.
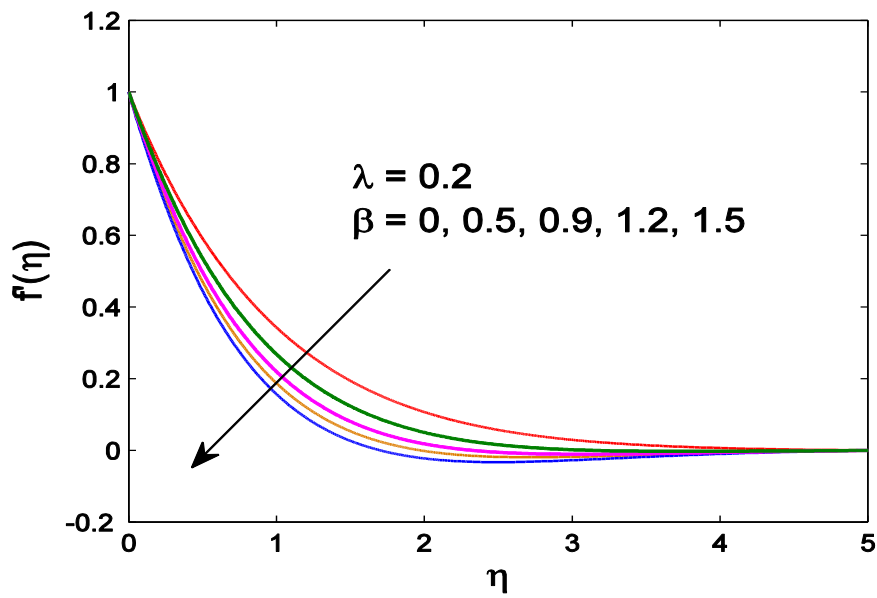

Fig. 3.3: Profile of velocity field f' for variousvalues of β.
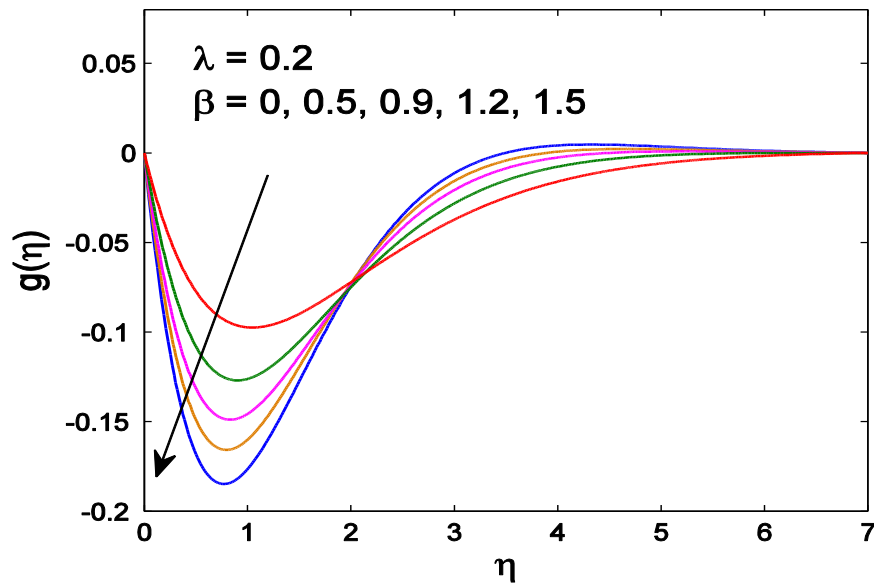
Fig. 3.4: Profile of velocity field g for various values of β.
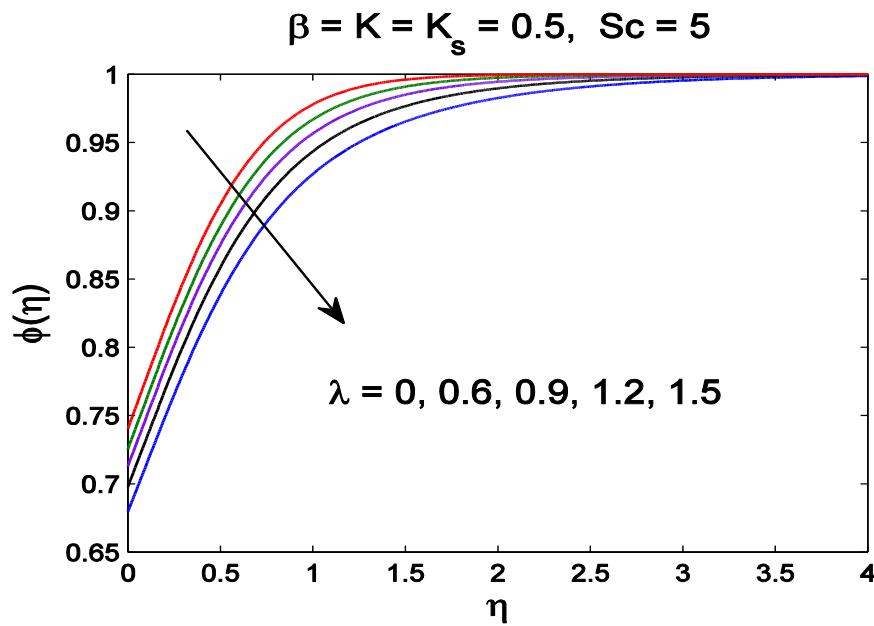
Fig. 3.5: Curves of concentration ϕ for various values of λ.
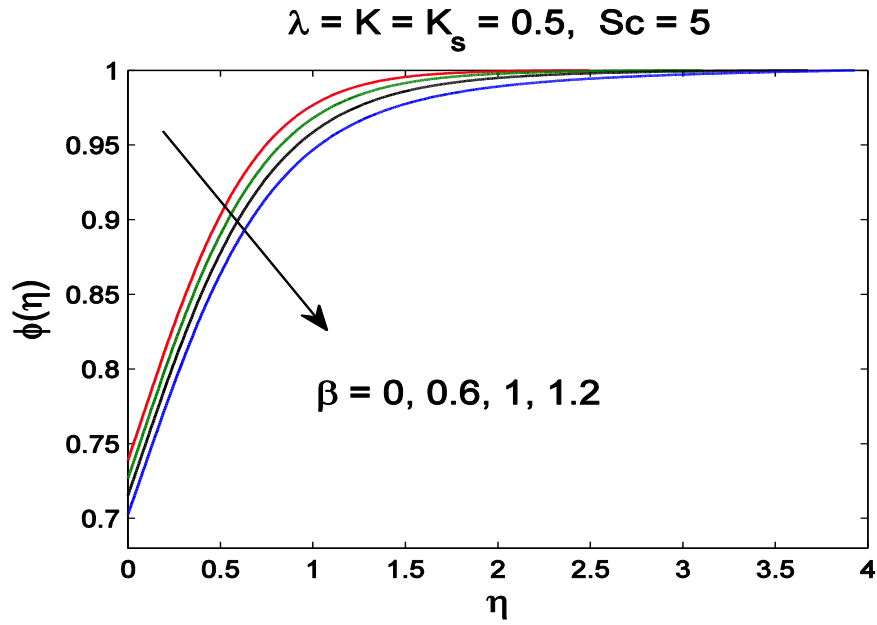
Fig. 3.6: Curves of concentration ϕ for various values of β.
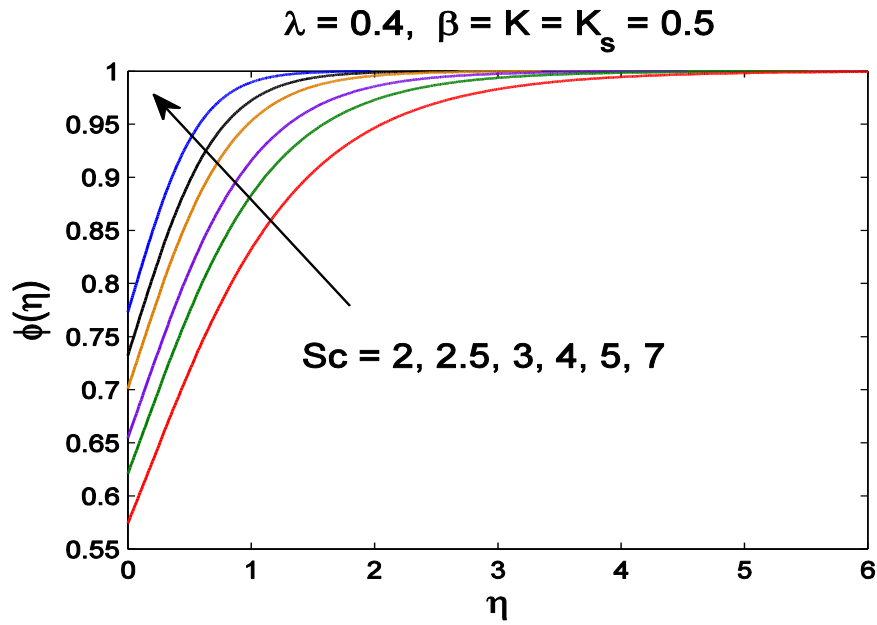
Fig. 3.7: Curves of concentration ϕ for various values of Sc.

λ = 0.4,   β = K_s = 0.5,   Sc = 5

φ(η)

K = 0.1, 1, 1.5, 1.9

η

Fig. 3.8: Curves of concentration ϕ for various values of K.

λ = 0.4,   β = K = 0.5,   Sc = 5

φ(η)

K_s = 0.5, 0.7, 1, 1.5, 2.5

η
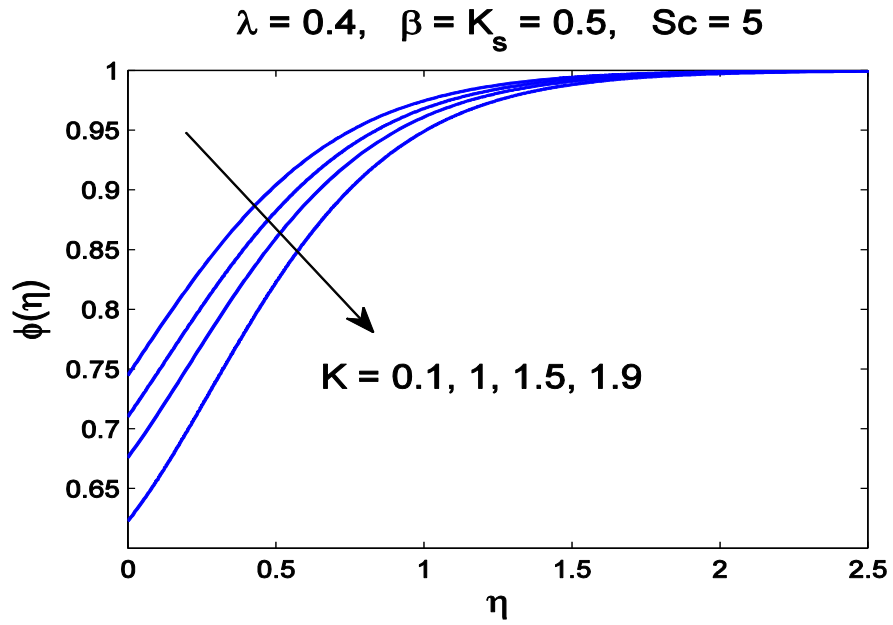
Fig. 3.9: Curves of concentration ϕ for various values of K_S.

Fig. 3.10: Profiles of surface concentration ϕ fordifferent values of K_s.

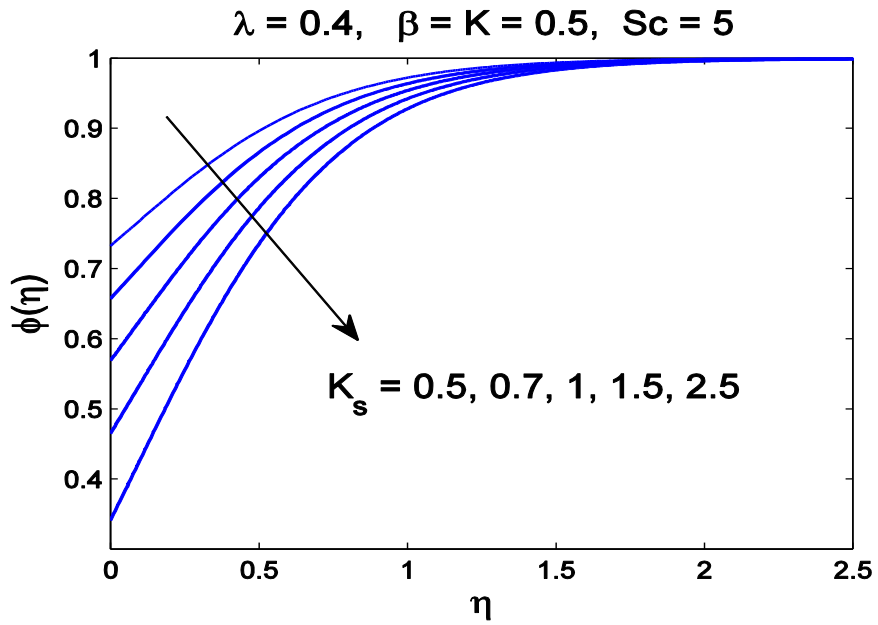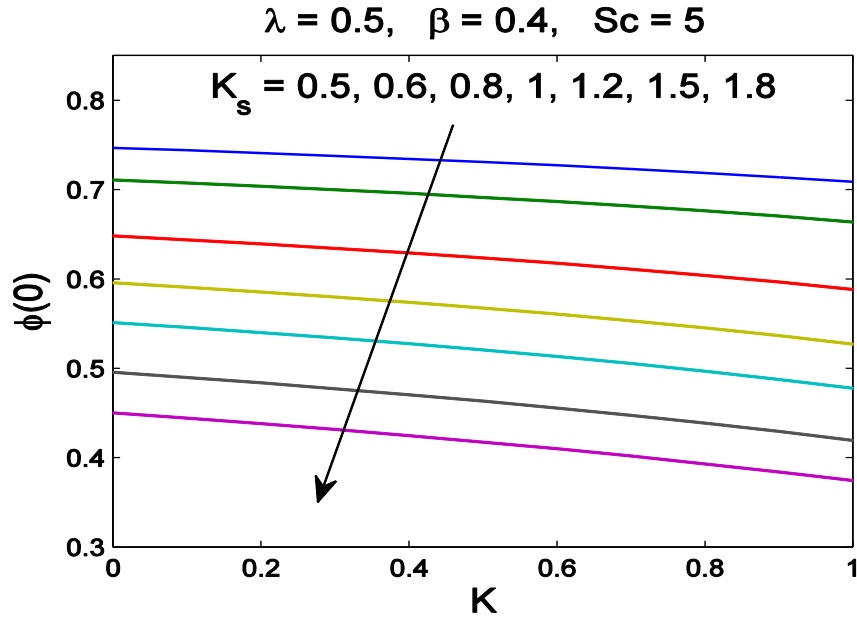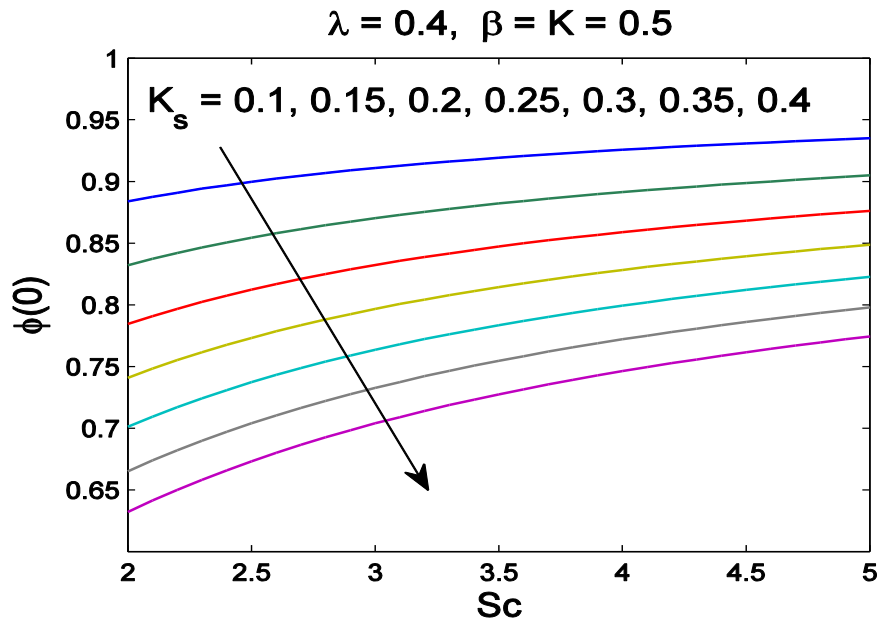Fig. 3.11: Profiles of surface concentration ϕ against the Schmidt number Sc.

Table 3.1: Comparison of computational results of $f''(0)$ with those of Nazar et al. [21] and Zaimi et al. [24] for different values of λ.

λ	$f''(0)$			$g'(0)$		
	Nazar et al. [21]	Zaimi et al. [24]	Present	Nazar et al. [21]	Zaimi et al. [24]	Present
0	-1.0000	-1.0000	-1.000000	0.0000	0.0000	0.000000
0.2	-	-1.0331	-1.033105	-	-0.2385	-0.238456
0.4	-	-1.1009	-1.100905	-	-0.4310	-0.430962
0.5	-1.1384	-1.1384	-1.138381	-0.5128	-0.5128	-0.512760
0.6	-	-1.1764	-1.176365	-	-0.5874	-0.587418
0.8	-	-1.2518	-1.251776	-	-0.7204	-0.720361
1	-1.3250	-1.3250	-1.325029	-0.8371	-0.8371	-0.837098
1.2	-	-1.3956	-1.395596	-	-0.9420	-0.941998
1.4	-	-1.4634	-1.463452	-	-1.0379	-1.037841
1.6	-	-1.5287	-1.528736	-	-1.1265	-1.126507
1.8	-	-1.5916	-1.591637	-	-1.2093	-1.209321
2	-1.6523	-1.6523	-1.652352	-1.2873	-1.2873	-1.287258
3	-	-1.9280	-1.928932	-	-1.6248	-1.624735
4	-	-2.1716	-2.171594	-	-1.9054	-1.905391
5	-	-2.3901	-2.390142	-	-2.1506	-2.150523

Table 3.2: Numerical values of $\phi'(0)$ for different values of $\lambda, \beta, Sc, K, K_s$.

λ	β	Sc	K	K_s	$-\phi'(0)$	
					Bvp4c	Shooting
0.1	0.5	1	0.5	0.5	0.227768	0.227769
0.2					0.218724	0.218725
0.3					0.203727	0.203727
0.4					0.179785	0.179785
0.2	0	1	0.5	0.5	0.240242	0.240243
	0.5				0.218724	0.218725
	1				0.187797	0.187798
	1.5				0.122353	0.122353
0.2	0.5	1	0.5	0.5	0.218724	0.218725
		2			0.297792	0.297792
		5			0.368815	0.368815
		7			0.388185	0.388185
		9			0.400811	0.400811
0.2	0.5	1	0.5	0.5	0.218724	0.218725
			1		0.075285	0.075284
			1.5		0.012587	0.012587
			2		0.019981	0.019981
0.2	0.5	1	0.5	1	0.275885	0.275886
				2	0.323082	0.323083
				5	0.365427	0.365427
				10	0.383701	0.383702

A model is constituted for homogeneous-heterogeneous reactions in the rotating flow of Maxwell fluid bounded by a linearly deforming surface. The arising similarity equations are tackled via shooting approach combined with RK-integration technique. The step size and tolerance of 10^{-3} and 10^{-6} are imposed in order to achieve accurate approximations. Table 3.1 presents a comparative study of our simulations for $f''(0)$ and $g'(0)$ with those of the existing articles in Newtonian limit ($\beta = 0$). The results match very well with those found byNazar et al. [21], Zaimi et al. [24] for full range of rotation-strength parameter λ. It is apparent that wall velocity gradients $f''(0)$ and$g'(0)$, which are proportional to the drag coefficient, enhance for large rotation-strength parameter. Table 3.2 provides computations for wall concentration gradient for various parameter values. For a check, the results are also evaluated through a contemporary subroutine bvp4c of MATLAB 2010. Table 3.2 demonstrates that both approaches yield almost identical solutions for certain range of parameters. The magnitude of $\phi'(0)$ decreases as parameter λ is incremented. It implies that fluid angular velocity contributes to a growth in wall slope of concentration. Moreover, we found a decreasing trend in $\phi'(0)$ for increasing values of Deborah number β. Also, a considerable enhancement in $\left|\phi'(0)\right|$ is found where large Schmidth number is employed.

Figs. 3.1 and 3.2 display the evolution of similarity profiles f' and g respecting $x-$and $y-$ components of velocity respectively for various choices of rotation-strength parameterλ. An increase in λ can be realized by either increasing rotation rate while maintaining constant stretch rate or by decreasing the stretch rate by keeping rotation rate constant. For smaller values ofλ, the change in f' with increasing η exponentially monotonic while it becomes non-monotonic when large λ is accounted. Indeed, both f' and g are oscillatory decaying functions of η when large rotation rate is consider. Similar conclusion was drawn in previous works [24]. It is investing to observe that function $g(\eta)$ is negative which illustrates that counter-clockwise fluid rotation includes fluid flow only in the negative $y-$direction. The reduction in f' or g with λ also indicates that boundary layer thickness has inverse relationship withλ.

For a specific rotation-strength parameterλ, the velocity curves f' and g are plotted for a variety of Deborah numbers in Figs. 3.3 and 3.4 respectively. With an increase in β, thecurves of f' and g exponentially decay at shorter distance from the wall. This illustrates that momentum penetration depth reduces with increasing elastic effect. Physically largerDeborah number

indicates that recovery process is slower and fluid behavior resembles to that of elastic solid substance. Consequently, fluid flow in both $x-$ and $y-$ directions decelerates and boundary layer thins as β increases. Similar behavior has also been observed by [31]. Furthermore, the parameter β has mixed behavior on the function $g(\eta)$.

Fig. 3.5 demonstrates the change in concentration ϕ as therotation-strength parameterλ is varied. A general trend of $\phi(\eta)$ is such that it has a finite value at the wall and asymptotically reaches to 1 as $\eta \to \infty$. We observe that ϕ decreases and concentration layer expands when fluid is subjected to larger rotation rate.

Fig. 3.6 captures the variation in concentration profile $\phi(\eta)$ when theDeborah number β is changed. For increasing values of β, solute concentration decreases while its profile becomes broader indicating a growth in concentration boundary layer thickness.

Fig. 3.7 shows the change inconcentration profile $\phi(\eta)$ as theSchmidt number Sc varies. An increasing trend in ϕ is depicted for increasing values of Sc. Howeverconcentration boundary layer shrinks upon increasing Sc. Physically, higher value of $Sc(=\frac{v}{D})$ implies smaller mass diffusion coefficient which give rise to shorterconcentration boundary layer.

Fig. 3.8 exhibits the behavior of parameter K, representing homogeneous reaction strength, on concentration profile $\phi(\eta)$. Concentration ϕ decreases whileconcentration boundary layer becomes thickerhomogeneous reaction strengthens.

Fig. 3.9 shows the development of concentration profiles for various values of heterogeneous (surface) reaction strength parameter K_s. With increasing strength of heterogeneous reaction, the concentration profile decreases in magnitude. It follows from the fact that an increase in either K or K_s leads to the consumption of reactants in the flow field due to which $\phi(\eta)$ decreases.

Fig. 3.10 shows the profiles of surface concentration $\phi(0)$ against parameter K for varying values of K_s. It is apparent that concentration at the surface decreases for increasing values of K_s. Interestingly, $\phi(0)$ varies linearly with K for all employed values of K_s. The variation in surface concentration $\phi(0)$ with Schmidt number Sc for different values of K_s is shown in Fig. 3.11. With an increment in Schmidt number Sc, the surface concentration $\phi(0)$ grows non-linearly and this growth increases in magnitude when bigger values of K_s are accounted.

Chapter 4

Concluding remarks

In this thesis, heat and mass transfer analysis is performed for rotating flow of Maxwell fluid. Heat transfer process is investigated in the existence of non-linear radiation. Also a model of homogeneous-heterogeneous reactions is explored. A numerical approach is adopted to tackle the governing similarity equations. The major implications of this research are explained below:

1. Velocity profiles decreases in the $x-$ and $y-$ direction by increasing the Deborah number γ.

2. Velocity components and local Nusselt number reduce when angular velocityΩ is increased.

3. Boundary layer thickness of temperature $\theta(\eta)$leads to an enhancementwhen temperature ratio parameter θ_w is incremented.

4. S-shaped curves of temperature $\theta(\eta)$ is examined when lager values of θ_w are considered.

5. When $A = -1$,temperature $\theta(\eta)$ has Sparrow-Gregg type Hills (SGHs) which shows that velocity profile moves towards the stretching sheet.

6. Slope of $\theta(\eta)$and wall heat transfer rate near the stretching sheet is larger for higher Prandtl number

7. Magnitude of heat transfer rate $-(1 + Rd\theta_w^3)\theta'(0)$ rises when values of A and θ_w are incremented.

8. Rotation-strength parameter λ has a retarding influence on velocity profiles. Concentration boundary layer expands when larger angular velocity is considered.

9. With increase Schmidt number, boundary layer becomes thinner and concentration distribution enhances in the boundary layer.

10. Concentration profile decreases with increasing strengths of homogeneous-heterogeneous reactions.

11. Counter-clockwise rotation sets up fluid flow in the negative $y-$direction which is apparent from the plots of $g(\eta)$ against η.

12. Surface concentration increases non-linearly with increasing Schmidt number Sc.

13. Current computations match very well with those of the existing literature in limiting cases.

References

1. K. Vajravelu, K.V. Prasad and A. Sujatha, Convection heat transfer in a Maxwell fluid at a non-isothermal surface, Central Eur. J. Phys. 9 (2011) 807-815.

2. K. L. Hsiao, MHD stagnation point viscoelastic fluid flow and heat transfer on a thermal forming stretching sheet with viscous dissipation, Canad. J. Chem. Eng. 89 (2011) 1228-1235.

3. S. Mukhopadhyay, Heat transfer analysis of the unsteady flow of a Maxwell fluid over a stretching surface in the presence of a heat source/sink, Chin. Phys. Lett. 29 (2012) Article ID: 054703.

4. T. Hayat, M. Mustafa, S. A. Shehzad and S. Obaidat, Melting heat transfer in the stagnation-point flow of an upper-convected Maxwell (UCM) fluid past a stretching sheet, Int. J. Numer. Methods Fluids 68 (2012) 233-243.

5. S. A. Shehzad, A. Alsaedi and T. Hayat, Hydromagnetic steady flow of Maxwell fluid over a bidirectional stretching surface with prescribe surface temperature and prescribed heat flux, PLoS One 8 (2013) Article ID: e68139.

6. M. Kumari and G. Nath, Steady mixed convection flow of Maxwell fluid over an exponentially stretching vertical surface with magnetic field and viscous dissipation, Meccanica 49 (2014) 1263-1274.

7. K. L. Hsiao, Conjugate heat transfer for mixed convection and Maxwell fluid on a stagnation point, Arab. J. Sci. Eng. 39 (2014) 4325-4332.

8. J. A. Khan, M. Mustafa, T. Hayat and A. Alsaedi, Numerical study of Cattaneo-Christov heat flux model for viscoelastic flow due to an exponentially stretching surface, PLoS One (2015) Article ID: 0137363.

9. M. Mustafa and A.Mushtaq, Model for natural convective flow of visco-elastic nanofluidpast an isothermal vertical plate, Eur. Phys. J. Plus130(2015) Article ID: 178,DOI: 10.1140/epjp/i2015-15178-1.

10. T. Hayat, B. Ashraf, S. A. Shehzad and N. Bayomi, Mixed convection flow of viscoelastic nanofluid over a stretching cylinder, J. Braz. Soc. Mech. Sci. Eng. 37 (2015) 849-859.

11. M. Mustafa, J. A. Khan, T. Hayat and A. Alsaedi, Simulations for Maxwell fluid flow past a convectively heated exponentially stretching sheet with nanoparticles, AIP Advances 5 (2015) Article ID: 037133, http://dx.doi.org/10.1063/1.4916364 .

12. M. Mustafa, J. A. Khan, T. Hayat and A. Alsaedi, Sakiadis flow of Maxwell fluid considering magnetic field and convective boundary conditions, AIP Advances 5 (2015) Article ID: 027106, http://dx.doi.org/10.1063/1.4907927 .

13. L. Cao, X. Si, L. Zheng and H. Pang, Lie group analysis for MHD effects on the convectively heated stretching porous surface with the heat source/sink, Bound Val Prob. 2015 (2015) Article ID: 63, DOI 10.1186/s13661-015-0326-4.

14. M. Mustafa, J. A. Khan, T. Hayat and A. Alsaedi, Simulations for Maxwell fluid flow past a convectively heated exponentially stretching sheet with nanoparticles, AIP Advances 5 (2015) Article ID: 037133, http://dx.doi.org/10.1063/1.4916364.

15. J. Li, L. Zheng and L. Lui, MHD viscoelastic flow and heat transfer over a verticle stretching sheet with Cattaneo-Christov heat flux effects, J. Mol. Liq. 221 (2016) 19-25.

16. M. Mustafa and J. A. Khan, Numerical analysis for Sakiadis flow problem considering Maxwell nanofluid, Therm. Sci. (2016), http://dx.doi.org/10.2298/TSCI150306001M.

17. A. Mushtaq, S. Abbasbandy, M. Mustafa, T. Hayat and A. Alsaedi, Numerical solution for Sakiadis flow of upper-convected Maxwell fluid using Cattaneo-Christov heat flux model, AIP Advances 6 (2016)) Article ID: 015208.

18. N. Khan, T. Mahmood, M. Sajid and M. S. Hashmi, Heat and mass transfer on MHD mixed convection axisymmetric chemically reactive flow of Maxwell fluid driven by exothermal and isothermal stretching disks, Int. J. Heat Mass Transf. 92 (2016) 1090-1105.

19. K. L. Hsiao, Combined electrical MHD heat transfer thermal extrusion system using Maxwell fluid with radiative and viscous dissipation effects, Appl. Therm. Eng. 112 (2017) 1281-1288.

20. C. Y. Wang, Stretching a surface in a rotating fluid, ZAMP 39 (1988) 177-185.

21. R. Nazar, N. Amin and I. Pop, Unsteady boundary layer flow due to a stretching surface in a rotating fluid, Mech. Research Comm. 31 (2004) 121-128.

22. M. Kumari, T. Grosan and I. Pop, Rotating flow of Power-Law fluids over a stretching surface, Tech. Mech. 26 (2006) 11-19.

23. T. Javed, M. Sajid, Z. Abbas and N. Ali, Non similar solution for rotating flow over an exponentially stretching sheet, Int. J. Numer. Meth. Heat Fluid Flow 21 (2011) 903-908.

24. K. Zaimi, A. Ishak and I. Pop, Stretching surface in rotating viscoelastic fluid, Appl. Math. Mech. 34 (2013) 945-952.

25. M. Turkyilmazoglu, MHD fluid flow and heat transfer due to a stretching rotating disk, Int. J. Therm. Sci. 51 (2012) 195-201.

26. M. Turkyilmazoglu, Bodewadt flow and heat transfer over a stretching stationary disk, Int. J. Mech. Sci. 90 (2014) 246-250.

27. M. Mustafa, J. A. Khan, T. Hayat and A. Alsaedi, on Bodewadt flow and heat transfer of nanofluid over a stretching stationary disk, J. Mol. Liq. 211 (2015) 119-125.

28. M. Mustafa, Cattaneo-Christov heat flux model for rotating flow and heat transfer of upper-convected Maxwell fluid, AIP Advances 5 (2015) Article ID: 047109, http://dx.doi.org/10.1063/1.4917306.

29. H. Rosali, A. Ishaq, R. Nazar and I. Pop, Rotating flow over an exponentially shrinking sheet with suction, J. Mol. Liq. 211 (2015) 965-969.

30. R. Ahmad and M. Mustafa, Model and comparative study for rotating flow of nanofluids due to convectively heated exponentially stretching sheet, J. Mol. Liq. 220 (2016) 635-641.

31. Z. Shafique, M. Mustafa and A. Mushtaq, Boundary layer flow of Maxwell fluid in rotating frame with binary chemical reaction and activation energy, Results in Physics 6 (2016) 627-633.

32. M. Mustafa, M. Wasim, T. Hayat and A. Alsaedi, A revised model to study the rotating flow of nanofluid over an exponentially stretching deforming sheet: Numerical solutions, J. Molec. Liq. 225 (2017) 320-327.

33. M. Mustafa, R. Ahmad, T. Hayat and A. Alsaedi, Rotating flow of viscoelastic fluid with non-linear thermal radiation: a numerical study, Neural Comput and Applic (2016), DOI 10.1007/s00521-016-2462-x.

34. M. A. Chaudhary and J. H. Merkin, Homogeneous-heterogeneous reactions in boundary-layer flow: Effects of loss of reactant, Math. Comp. Model. 24 (1996) 21-28.

35. J. H. Merkin, A model for isothermal homogeneous-heterogeneous reactions in boundary-layer flow,Math. Comp. Model. 24 (1996) 125-136.

36. N. Bachok, A. Ishak and I. Pop, On the stagnation-point flow towards a stretching sheet with homogeneous-heterogeneous reactions effects, Commun. Non-Lin. Sci. Numer. Simulat. 16 (2011) 4296-4302.

37. S. Shaw, P. K. Kameswaran and P. Sibanda, Homogeneous-heterogeneous reactions in micropolar fluid flow from a permeable stretching or shrinking sheet in a porous medium, Bound Val Prob. 2013 (2013) Article ID: 77.

38. P. K. Kameswaran, S. Shaw, P. Sibanda and P.V.S.N Murthy, Homogeneous-heterogeneous reactions in a nanofluid flow due to a porous stretching sheet, Int. J. Heat Mass Transf. 57 (2013) 465-472.

39. T. Hayat, M. Imtiaz and S. Almezal, Modeling and analysis for three-dimensional flow withhomogeneous-heterogeneous reactions, AIP Advances 5 (2015) Article ID: 107209, http://dx.doi.org/10.1063/1.4933084 .

40. T. Hayat, M.Imtiaz and A. Alsaedi, MHD flow of nanofluid with homogeneous-heterogeneous reactions and velocity slip, Therm. Sci. (2015) DOI: 10.2298/TSCI140922067H (2015).

41. T. Hayat, M. Imtiaz andA. Alsaedi, Effects of homogeneous-heterogeneous reactions in flow of Powell-Eyring fluid, J. Cent. South. Univ. 22 (2015) 3211-3216.

42. M. Ramzan, M. Bilal and J. D. Chung, Effects of MHD homogeneous-heterogeneous reactions on third grade fluid flow with Cattaneo-Christov heat flux, J. Molec. Liq. 223 (2016) 1284-1290.

43. M. Radiah and R. Kandasamy, Homogeneous-heterogeneous reactions of the water based Cu, Al_2O_3 and SWCNTs on MHD stagnation-point flow over stretching/shrinking sheet with generalized slip condition, Chem. Process Eng. Research 42 (2016) 2225-0913.

44. A.Raptis , Radiation and free convection flow through a pourous medium, Int. Commun Heat Mass Transfer 25 (1998) 289-295.